



Sensitivity of the Eocene Climate to CO₂ and Orbital Variability

John S. Keery¹, Philip B. Holden¹, Neil R. Edwards¹

¹School of Environment, Earth & Ecosystem Sciences, The Open University, Milton Keynes, MK7 6AA, UK

Correspondence to: John S. Keery (john.keery@open.ac.uk)

5 **Abstract.** The early Eocene, from about 56 Ma, with high atmospheric CO₂ levels, offers an analogue for the response of the Earth's climate system to anthropogenic fossil fuel burning. In this study we present an ensemble of 50 Earth system model runs with an early Eocene palaeogeography and variation in the forcing values of atmospheric CO₂ and the Earth's orbital parameters. Two-dimensional model output fields are reduced to scalar values through simple summarising algorithms and by singular value decomposition. Relationships between these scalar results and the forcing parameters are identified by
10 linear modelling, providing estimates of the relative magnitudes of the effects of atmospheric CO₂ and each of the orbital parameters on important climatic features, including tropical-polar temperature difference, ocean-land temperature contrast, and Asian, African and S. American monsoon rains. Our results indicate that although CO₂ exerts a dominant control on most of the climatic features examined in this study, the orbital parameters also strongly influence important components of the ocean-atmosphere system in a greenhouse Earth. In our ensemble, atmospheric CO₂ spans the range 280 - 3000 ppm,
15 and this variation accounts for over 95% of the effects on mean air temperature, southern winter high-latitude ocean-land temperature contrast and northern winter tropical-polar temperature difference. However, the variation of precession accounts for over 75% of the influence of the forcing parameters on the Asian and African monsoon rainfall, and obliquity variation accounts for over 65% of the effects on winter ocean-land temperature contrast in high northern latitudes. Our method gives a quantitative ranking of the influence of each of the forcing parameters on key climatic model outputs, with
20 additional spatial information from our singular value decomposition approach providing insights into likely physical mechanisms. The results demonstrate the importance of orbital variation as an agent of change in climates of the past.

1 Introduction

In the early Eocene several episodes of global warming coincided with carbon isotope excursions (CIEs), pulses of isotopically light carbon injected into the atmosphere and oceans, and recorded in high-resolution marine and terrestrial
25 sediments (Kennett and Stott, 1991). In one large CIE, at the Palaeocene-Eocene transition at ~56 Ma, the Palaeocene-Eocene Thermal Maximum (PETM), evidence from both tropical (e.g. Zachos et al., 2003) and polar (e.g. Sluijs et al., 2006) regions indicates that temperatures increased by ~5°C in less than 10 kyr. Although the greenhouse gas (GHG) sources, and the duration of the onset phase of the PETM are uncertain, the relatively short time scale and global extent of the PETM strongly suggest that a large and sudden increase in GHGs in the atmosphere was the primary climatic forcing factor (Zachos



et al., 2007). Since estimates of GHG emissions during the PETM are similar in magnitude to present-day emissions produced by fossil fuel burning, the PETM may provide a valuable analogue for anthropogenic climate change (e.g. McInerney and Wing, 2011; Zeebe and Zachos, 2013).

The CIEs of the early Eocene show similar regularity in their timing to periodic changes in the Earth's orbit around the sun (Lourens et al., 2005), and the search for causal relationships between orbital cycles and Paleogene climate is an active area of research (e.g. Lauretano et al., 2015; Laurin et al., 2016; Lunt et al., 2011).

Although the climatic state in the early Eocene cannot be directly measured, much information on temperature and biogeochemical conditions can be inferred from measurements of proxy data: preserved natural records of climate variability, which can be linked to the property of interest through physical processes (Jones and Mann, 2004). But there are major uncertainties in proxy data from the Eocene due to incomplete preservation and alteration over time, with additional uncertainties as to the seasonality of contributory processes, and for ocean proxies, the depth at which the property of interest, e.g. temperature, influences the proxy (Dunkley Jones et al., 2013). Climate models therefore have an important role to play in exploring the mechanistic functioning of palaeoclimates (Huber, 2012).

Climate simulations with high temporal and spatial resolution can be obtained from General Circulation Models (GCMs), but the requirement of GCMs for powerful computers and long run-times precludes their use in large ensembles of model simulations and restricts their ability to investigate the large uncertainties in forcings and model parameterisations. Such ensembles are more practical with more heavily parameterised and hence more computationally efficient Earth system Models of Intermediate Complexity (EMICs), (Weber, 2010).

In this study we deploy an EMIC, PLASIM-GENIE (Holden et al., 2016), in an ensemble of model runs to investigate the effects of varying GHG concentration and orbital parameters on the palaeoclimate of the Earth, with an Eocene configuration of the oceans and continents. We reduce the dimensionality of the model output by computing simple scalar metrics to denote key climatic features of each ensemble member, and we apply singular value decomposition (SVD) to identify the principal components (PCs) of temperature and precipitation fields in the full ensemble, for comparison with the variation in the forcing parameters.

By applying the linear modelling method of Holden et al. (2015), we regress both the simple scalar metrics and the SVD reduced dimension model outputs onto the forcing parameters, and from the derived relationships, we infer main effects indices denoting the effect of each explanatory term, and total effect indices denoting the effect of each forcing parameter, on the variation in the scalar metrics and on the temperature and precipitation output fields.

2 The Early Eocene and the PETM

During the Eocene, the Earth remained in the 'greenhouse' state, which had persisted since the early Cretaceous, with polar air temperatures remaining above 0°C for most of the year (Wing and Greenwood, 1993), no permanent polar ice-caps, reduced equator-pole temperature gradients, and lower ocean-land temperature contrasts, inferred from fossil and isotope



indicators of temperature and environmental conditions. Climate modellers have experienced difficulty in simulating Cretaceous and Palaeogene 'equable climates' (Sloan and Barron, 1990; Wing and Greenwood, 1993) with sufficient warming at high latitudes, without overheating the tropics, although Huber and Caballero (2011), hereafter HC11, have demonstrated that with sufficiently high levels of radiative forcing, climate models can generate global air temperature distributions in broad agreement with the proxy temperature measurements.

The onset of the PETM, at approximately 55.9 Ma (Westerhold et al., 2009), is recognised as the boundary between the Palaeocene and Eocene epochs (Aubry et al., 2007), and is characterised by a large CIE, indicating large GHG emissions, accompanied by a sudden rise in global temperature (Kennett and Stott, 1991), extensive extinction and origination of nannoplankton (Gibbs et al., 2006), and widespread ocean anoxia (Dickson et al., 2012). There is some evidence that some of the GHG emissions were initially in the form of CH₄, which is oxidised in the atmosphere to CO₂ (Dickens, 2011; Lunt et al., 2011). The PETM is also marked by enhanced precipitation and continental weathering (Carmichael et al., 2016; Chen et al., 2016; Penman, 2016), rapid and sustained surface ocean acidification (Penman et al., 2014; Zachos et al., 2005), and shares many features of the global-scale oceanic anoxic events of the Cretaceous and Jurassic periods (Jenkyns, 2010). See McInerney and Wing (2011) for a review of PETM research.

The duration of the onset phase of the PETM is uncertain. Cui et al. (2011) have suggested that the peak rate of addition of CO₂ to the atmosphere was much lower than the present-day rate of anthropogenic GHG emissions, but this is disputed by Sluijs et al. (2012). Zeebe et al. (2016) have estimated that the initial release of carbon at the onset of the PETM lasted at least 4 Ka, at a rate which was little more than one tenth of the present rate of anthropogenic emissions, so the Earth may already be in a 'no-analogue' state, with anthropogenic climate change likely to exceed that of the PETM. However rapid the onset, the greenhouse conditions of the early Eocene, and particularly the PETM, provide an opportunity to apply lessons from the past, with a view to improving predictions of the future (Lunt et al., 2013).

2.1 Palaeogeography of the Early Eocene

Although the arrangement of the continents and oceans in the Early Eocene was broadly similar to that of the present, tectonic movements may have effected some changes to the climate system. In particular, the configuration of ocean gateways strongly influences modes of ocean circulation, and hence affects energy transport throughout the climate system (Lunt et al., 2016; Sijp et al., 2014).

2.1.1 Continental and Ocean Configurations during the Early Eocene

Although the Bering Strait was closed throughout the Palaeogene (Marincovich et al., 1990), and the Western Interior Seaway linking the Arctic to the Pacific was closed by the end of the Cretaceous (Slattery et al., 2015), the Arctic Ocean was connected to the major oceans during the early Eocene through the Turgai Strait, also known as the Western Siberian Seaway (Akhmetiev et al., 2012; Radionova and Khokhlova, 2000). The Lomonosov Ridge, from which core samples have been obtained by the Arctic Coring Expedition (ACEX) of the Integrated Ocean Drilling Program Expedition (IODP) 302



(Backman et al., 2008), was on the edge of the Arctic basin rather than across the pole as in the present configuration (O'Regan et al., 2008).

Both the Drake Passage between South America and Antarctica (Barker and Burrell, 1977) and the Tasman Gateway between Australia and Antarctica (Exon et al., 2004) were closed during the early Eocene, preventing the development of an Antarctic Circumpolar Current and allowing greater southern hemisphere meridional heat transport than in the modern world.

2.1.2 Orbital Configurations

Throughout Earth's geological history, oscillations in the relative positions of the Earth and Sun have influenced both the Earth's climate, and rates of sedimentation in some climate-sensitive environmental settings (Hinnov and Hilgen, 2012). The main oscillations are the eccentricity of the Earth's orbit around the Sun, with dominant periods of ~100 ka and ~400 ka, the obliquity or tilt of the Earth's axis of rotation, with a period of ~40 ka, and precession, the relative timing between perihelion and the seasons, with a period of ~20 ka (Berger et al., 1993). By correlating oscillations preserved in the geological record with computed time series of changes in insolation received by the Earth, an absolute astronomical time scale may be constructed for recent time-spans with a complete sedimentary record, but where the geological evidence is incomplete, or where uncertainties in the orbital model are too great further back in time, only a relative time scale may be derived (Hilgen et al., 2010). An absolute astronomical time scale has been computed back to 50 Ma (Laskar et al., 2011), and an absolute age of 55.53 ± 0.05 Ma has been proposed for the onset of the PETM at the start of the Eocene epoch by Westerhold et al. (2012).

Lourens et al. (2005) noted the apparent astronomical pacing of global warming events in the late Palaeocene and early Eocene, with correlations to both the long and short periods of eccentricity. Sexton et al. (2011) suggested that although the smaller hyperthermal events of the early Eocene were driven by cycles of carbon sequestration and release in the ocean, paced by the eccentricity cycles, the PETM was likely to have been driven by carbon injection from a sedimentary source. Laurin et al. (2016) applied a method which allows the phase of the ~400 Ka eccentricity cycle to be identified from interference patterns and frequency modulation of the ~100 Ka eccentricity cycle, and concluded that four hyperthermals in the early Eocene were initiated at ~400 Ka eccentricity maxima, but in a study of terrestrial sediments with apparent correlation to the ~100 Ka eccentricity cycle, Smith et al. (2014) suggested that hyperthermals occurred during eccentricity minima, rather than maxima.

Ruddiman (2006) noted a relationship between obliquity and the extent of northern ice sheets, and also some correlation between precession and northern summer monsoons, but this was thought to be related to feedbacks in the growth and decay of ice-sheets, and so may not be pertinent to the climate of the Eocene.



3 The PLASIM-GENIE Model

PLASIM-GENIE (Holden et al., 2016) is an intermediate complexity AOGCM. We apply the model at T21 atmospheric resolution with 10 layers, and a matching ocean grid with 32 depth levels. We apply the calibrated parameter set of Holden et al (2016). The component modules are as follows:

PLASIM (Fraedrich, 2012) is built around the 3D primitive equation atmosphere model PUMA (Fraedrich et al., 2005). The radiation scheme considers two wavelength bands in the short wave and uses the broad band emissivity method for long wave. Fractional cloud cover is diagnosed. Other parameterised processes include large-scale precipitation, cumulus and shallow convection, dry convection and boundary layer heat fluxes.

GOLDSTEIN is a 3D frictional-geostrophic ocean model (Edwards and Marsh, 2005; Marsh et al., 2011), dynamically similar to classical GCMs, except that it neglects momentum advection and acceleration. Barotropic flow around the four continental islands (Fig. 1) is derived from linear constraints that arise from integrating the depth-averaged momentum equations.

GOLDSTEINSEAICE (Edwards and Marsh, 2005) solves for the fraction of the ocean surface covered by ice within a grid cell and for the average sea-ice height. A diagnostic equation is solved for the ice surface temperature. Growth or decay of sea ice depends on the net heat flux into the ice (Hibler III, 1979; Semtner Jr, 1976). Sea-ice dynamics are represented by diffusion and advection by surface currents.

ENTS (Williamson et al., 2006) models vegetative and soil carbon densities, assuming a single plant functional type. Photosynthesis depends upon temperature (with a double-peaked response representing boreal and tropical forest), atmospheric CO₂ concentration and soil moisture availability. Self-shading is parameterised. Land surface albedo, moisture bucket capacity and surface roughness are parameterised in terms of the simulated carbon pool densities.

4 Methods

4.1 Model Configuration

4.1.1 Model Grid

Herold et al. (2014) published a high-resolution dataset of Eocene palaeogeography, which we have used as an initial configuration for the tectonic layout, topography and bathymetric boundary conditions in our study. We have reduced the resolution of the Eocene palaeogeography provided by Herold et al. (2014) to a configuration of 64 longitude x 32 latitude cells, with each cell representing 5.625° in each orientation. Cells at high latitudes therefore represent smaller land areas than cells at low latitudes. Our vertical resolution is 32 ocean depths and 10 atmospheric layers. We have incorporated the ocean gateway configurations discussed in section 2.1.1. The Turgai Strait is open in our configuration, and is the only connection between the Arctic Ocean and other oceans. The Drake Passage and Tasman Gateway are both closed.



The palaeogeography (Fig. 1) comprises four land masses: N America and Eurasia; Antarctica combined with S America and Australia; Africa; and India. Red rectangles in Fig. 1 indicate the boundaries of areas used to calculate simple metrics of centennially averaged seasonal precipitation, as empirical indicators of African, Asian and S. American monsoons.

4.1.2 Forcing and Other Input Parameters

5 In order to investigate the sensitivity of the Eocene climate to variation in atmospheric CO₂ and orbital parameters, we have constructed an ensemble of 50 model configurations, each with a unique set of forcing parameters comprising atmospheric CO₂, eccentricity, obliquity and precession, with an additional dummy parameter included to test for possible overfitting of relationships between forcing parameters and model output fields.

Although the maximum value of CO₂ injected into the atmosphere during CIEs, and in particular the PETM, remains
10 uncertain, there is broad agreement that it did not exceed 3000 ppm (e.g. Gehler et al., 2016), and that it did not fall below the pre-industrial level of 280 ppm at any time during the early Eocene. We allocate these values as the limits of a uniform range from which our ensemble of CO₂ values is selected.

Since the absolute astronomical time scale for the early Eocene has an uncertainty which is greater than the periods of the obliquity and precession cycles, and there remains disagreement as to which phases of the eccentricity cycles are related to
15 CIEs, we select values of orbital parameters independently, and from the full range of each parameter's variation during the early Eocene.

To ensure the best coverage of the five-dimensional state-space comprised of the four forcing parameters and the additional dummy parameter in a limited number of model runs, we apply the Latin hypercube method (McKay et al., 1979), a constrained Monte Carlo sampling scheme in which the range to be sampled for each variable is divided into non-
20 overlapping intervals, and one value from each interval is randomly selected (Wyss and Jorgensen, 1998). This provides adequate coverage of the state space more efficiently than can be achieved by a simple Monte-Carlo sampling approach (Rougier, 2007). Uniform ranges for each of the forcing parameters and the dummy parameter are shown in Table 1.

The intensity of radiation emitted by the Sun has increased steadily over time, and we apply the linear model of Gough (1981), and select a solar constant of 1358.68 W m⁻² Gough (1981).

25 4.1.3 Running the Models

Each simulation was run for 1000 years to reach a quasi-steady state, with key output fields recorded as seasonal averages for each of the three-month periods December, January and February (DJF) and June, July and August (JJA), representing both winter and summer seasons in both the northern and southern hemispheres. Although model output includes time series of some fields and output values every 100 years, in this study only the field values recorded at the end of the 1000 years of
30 modelling are used for analysis of the results.



4.2 Analysis of Model Output

Comparison of the forcing parameters applied in the ensemble with the model output fields can be more efficiently achieved by reducing the dimensionality of the model output while retaining information on key components of the climate system.

4.2.1 Simple Metrics

5 In studies of the Earth's modern climate, it is recognised that the tropical-polar temperature difference (TPTD) influences poleward energy flux, and the ocean-land temperature contrast (OLC) affects monsoon intensity (Jain et al., 1999; Karoly and Braganza, 2001; Peixoto and Oort, 1992). Although atmospheric circulation patterns in the early Eocene are likely to have differed from those in the modern world, in selecting latitude regions to represent the TPTD, we adopt the approach of Abbot and Tziperman (2008), who configured their model of the Cretaceous climate with latitude ranges of 0–30°, 30–60°,
10 and 60–90°, the approximate boundaries of the Hadley, Ferrel and Polar cells observed in the modern world (Peixoto and Oort, 1992). On our model grid in which each cell spans 5.625° of latitude, for the purposes of deriving scalar metrics, we define the tropical regions to be between 0.0° and 33.75° North and South, and the polar regions to be between 56.25° to 90° North and South.

15 From the output values of air temperature in the lowest level of the atmosphere, weighted by grid cell area, we derive scalar values for each model run, of global annual mean air temperature (MAT), northern and southern hemisphere seasonality (mean area-weighted DJF-JJA temperature differences in the above-defined polar regions), TPTD for summer and winter in each hemisphere, and ocean-land temperature contrast for summer and winter in tropical and polar regions in each hemisphere.

20 Monsoons are related to seasonal variations in tropical and subtropical winds and precipitation (Trenberth et al., 2006). Wang and Fan (1999) noted that the choice of an index to denote monsoon behaviour in the modern world is difficult and arbitrary, with commonly applied indices based on average summer precipitation, maximum summer precipitation, winter-summer difference in precipitation, or wind circulation patterns within defined geographical areas. In this study, we derive simple scalar metrics to denote indices for monsoons for Asia, Africa and South America from the difference in rainfall in DJF and JJA, for defined geographical regions, denoted on Fig. 1, and selected for their similarity to monsoonal regions in
25 the modern continental configuration.

4.2.2 Singular Value Decomposition and Model Emulation

We apply the linear algebraic tool SVD to identify the PCs and empirical orthogonal functions (EOFs) of temperature and precipitation fields in the full ensemble. A detailed presentation of the use of this method in the analysis of climate data is given by Hannachi (2004).

30 We use the linear modelling method of Holden et al. (2015), to regress both the simple scalar metrics and the SVD reduced dimension model outputs onto the forcing parameters. Values of the forcing parameters CO₂, eccentricity and obliquity



(with its very small angular range considered to be approximately linear) were normalised to the same range [-1, 1] as the sines and cosines of precession values, to form a 50-element column vector for each forcing factor. Each 2-D (32 x 64) result field for each ensemble member was unrolled to form a column vector of 2048 elements, comprising a single column within a 2048 x 50 matrix of full ensemble values.

- 5 SVD was applied to decompose the full ensemble matrix for each 2-D result field, providing a 2048 x 50 matrix of PCs, a 50 x 50 matrix of PC scores, and a 50 x 50 matrix of diagonal values.

Linear modelling was applied to determine relationships between the normalised forcing factors and the first six columns of the PC scores, including products of pairs of forcing factors, and squares of each forcing factor, with the best fitting relationships selected according to the Akaike information criterion then refined using Bayes information criterion. The resulting relationship provides a simple emulator which can be used to estimate a PC score for the 2-D model field, given a single set of forcing parameter values. Applying derived emulators in respect of temperature and precipitation for both seasons, demonstrated high correlation between emulated PC scores and PC scores derived directly through SVD (Table 2). A similar emulator approach has been applied by Bounceur et al. (2015) in a study of the response of the climate-vegetation system in interglacial conditions to astronomical forcing. Total effects indices, which denote the effect of each forcing parameter on the full-ensemble variation in the scalar metrics and on the temperature and precipitation output fields, are inferred from the derived relationships.

5 Results

Analysis of the model results has focused on variation in surface air temperature and precipitation in both winter and summer in each hemisphere. In the left column of Fig. 2, median temperatures at each grid cell for the full ensemble are plotted for DJF (top) and for JJA (bottom), with the standard deviations plotted in the right column.

Ranges of median temperatures over land are greater than over the oceans, but TPTD is smaller in both seasons and both hemispheres than simulated in the modern world (see Fig. 2, Holden et al 2016). It is apparent from the standard deviation field that the tropical-polar temperature difference varies substantially across the ensemble, particularly in northern winter. The temperature distributions are similar to those of the 2240 ppm CO₂ simulation of HC11, regarded as their “mid to late Eocene” analogue (they consider elevated CO₂ as a proxy for all radiative forcing, including uncertain climate sensitivity). The principal difference is in high northern latitude winter temperatures; the Arctic ocean remains above freezing in HC11. We note that the Arctic winter median temperature is below freezing in the PLASIM-GENIE ensemble, (see SST plots in Fig 3) and the Arctic does not remain ice-free throughout the year in any of the 50 simulations in our study. Tropical temperatures in excess of 35°C were simulated in some cases, as in HC11, which they regarded as their “most troubling result”, although they note observational data is currently insufficient to rule this out. Finally, we note that multi-model ensembles have found significant inter-model differences including, for instance a 9°C spread in global average temperature



under the same CO₂ forcing (Lunt et al 2012). A future analysis of PLASIM-GENIE parametric uncertainty is anticipated, but beyond the scope of this paper.

Full ensemble distributions of mean latitudinal distributions of annual mean sea surface temperature (SST), with mean latitudinal distributions of maritime and continental surface air temperature in both DJF and JJA are plotted in Fig. 3, together with ensemble medians and 5% and 95% percentiles of global annual mean SST, and maritime surface air temperature in both DJF and JJA. The greater range of temperatures below rather than above median values reflects our use of a uniform range of CO₂ forcing values, and the logarithmic response of temperature to increasing CO₂ concentration. There is substantial variation of mean temperature across the ensemble, around 20 degrees over land, but the temperature offset varies little with latitude outside of polar regions where snow and ice greatly reduce winter temperatures in the colder simulations. The variation in TPTD across the ensemble thus appears to be essentially driven by the strength of snow and ice albedo feedbacks.

Our ensemble distributions of sea and air temperatures are in broad agreement with the values from the Eocene model studies compared by Lunt et al. (2012) and with the tables of marine and terrestrial proxy data compiled by Lunt et al. (2012) and HC11, but it should be noted that these proxy data spanned the entire Eocene era. Our palaeogeography specifically represents the early Eocene, but our range of CO₂ and orbital inputs is more representative of the variation in forcing across the whole era.

Median values and standard deviations of precipitation at each grid cell are plotted in Fig. 4. Higher precipitation values and variation are largely confined to the tropics, especially to regions associated with monsoons in the present day: Africa and S. America in DJF, and S.E. Asia in JJA.

In Figs. 5 and 6, CO₂, obliquity and precession index are plotted against MAT, northern seasonality, northern winter TPTD and northern summer TPTD (Fig. 5), and southern winter polar OLC, northern winter polar OLC, Asian monsoon index and African monsoon index (Fig. 6). The dominant effect of CO₂ on MAT and northern seasonality is apparent in Fig. 5, and it can also be seen that CO₂ strongly affects the northern TPTD in the winter, but not in the summer, when the combined influence of obliquity and precession index is discernible, suggesting that temperature proxies with seasonal bias may have a significant orbital imprint. The plot of atmospheric CO₂ against N. Winter TPTD shows a change in gradient at approximately 1000 ppm CO₂ and 32°C. This may be related to the logarithmic dependence of radiative forcing on CO₂ concentration, as well as the disappearance of ice above some threshold level, cf Fig. 3.

It can be observed in Fig. 6 that there is strong correlation between CO₂ and southern winter polar OLC. The African and Asian monsoon indices are both correlated with the precession index, a well established feature of Quaternary records (e.g. Cruz et al., 2005). In each of these examples, there is no apparent correlation between the simple metric and two of the three forcing factors. We have selected these simple metrics with visible correlations to the forcing parameters for further analysis with the linear modelling and emulation methods. Total effects on the simple metrics have been calculated for each of the forcing parameters, with eccentricity and precession considered separately, rather than combined within the precession index, and are shown in Table 3.



The total effects of CO₂ on MAT, northern winter TPTD and southern winter polar OLC are all very high (> 0.95), and the total effects of obliquity on northern winter polar OLC, and of precession on both the Asian and African monsoon indices are all fairly high (> 0.65), providing quantitative confirmation of the correlations visible in Figs. 5 and 6.

Figure 7 shows the first three PCs of surface air temperature in DJF and JJA, with the percentages of temperature variation explained by each PC. Each of these plots illustrates the PC scaled by the standard deviation of the PC scores, thereby reflecting the variability across the ensemble. Note the variable scales for each of the subplots. In both DJF and JJA, PC1 explains over 95% of the variance, with TPTD clearly visible in both hemispheres in DJF, but apparent only in the southern hemisphere in JJA. OLC is apparent in the plots of PC1 in both DJF and JJA. OLC is discernible in PC2 for DJF temperature, which explains 2.4% of variance, but less apparent, at least in the southern hemisphere, for JJA temperatures, in which PC2 explains 2.6% of the variance. For temperature in both DJF and JJA, PC3 explains less than 1% of the variance, with some indication of TPTD and OLC in DJF, but only of weak OLC at high latitudes in JJA. It is worth noting that even though lower order PCs explain small percentages of global variances, these PCs are generally associated with specific regions where they are comparably important to the first PC.

In their presentation of the SVD method applied in this study, Holden et al. (2015) investigated the effects of orbital parameters on the Earth's climate in the present day, but without including CO₂ as a forcing parameter in their ensemble, and found that obliquity had a dominant effect on the PC score of annual average surface air temperature. In our study of the Eocene climate, CO₂ is strongly correlated with N. seasonality (Fig. 5), and obliquity is weakly correlated with TPTD in JJF (Fig. 5) and with OLC in DJF (Fig. 6). The first three PCs of precipitation in DJF and JJA are shown in Fig. 8. PC1 explains approximately 55% of the variance in both seasons, with PC2 and PC3 explaining over 20% and over 5% respectively, in both seasons. In both PC2 and PC3, areas of high seasonal contrast appear to correspond to areas which experience monsoons in the modern world.

Correlations between the PC scores of temperature and precipitation are provided in Table 4. The first PC scores of temperature, reflecting a global warming signal, are highly correlated with the first PC scores for precipitation, suggesting that these PCs reflect a strengthening of the hydrological cycle in response to warming. Similar considerations reveal connections between lower order PC scores, though we note that the 2nd (3rd) component of DJF temperature is associated with the 3rd (2nd) component of DJF precipitation. In order to address the drivers of these modes, we first consider the correlation coefficients, r , between forcing factors and the PC scores, shown in Table 5. These demonstrate that for each output there is a mode of variability driven by CO₂ and another mode driven by precession, suggesting they reflect global warming (and associated hydrological strength) and precessional forcing of the monsoon system.

There is strong correlation ($r^2 > 0.5$) between CO₂ and the first PC scores of temperature in DJF and JJA. There are also strong correlations between precession index and the third PC scores for DJF temperature, and between precession index and the second PC scores for JJA temperature.

CO₂ is strongly correlated with the first PC scores of precipitation in both DJF and JJA, and there is a strong relationship between precession index and the second PC scores of precipitation in both DJF and JJA.



The relationships between the forcing parameters and the simple metrics, and between the forcing parameters and the PC scores of 2-D fields, derived through linear modelling, include first and second order terms of forcing factors, together with products of forcing factors. In all cases most of the effects are confined to the first order terms, and in no case does eccentricity have a significant effect independently of precession, the effect of which eccentricity always augments slightly.

5 In Fig. 9, we therefore neglect the higher order terms and plot the emulator coefficients of the first order terms (also termed the 'main effects') of the forcing parameters on the first three PCs of temperature and precipitation for DJF. Figure 10 shows the main effects of the forcing parameters on the first three PCs of temperature and precipitation plotted for JJA.

In both seasons, PC1 for temperature and precipitation can be almost entirely explained by CO₂, reinforcing the earlier conclusion that these describe a connected mode, global warming with associated effects on the hydrological cycle. The main effects also suggest connections between the modes of variability of temperature and precipitation in lower-order components. In both seasons, and apparent in both variables, there is a mode that is driven by precession; we interpret this as a monsoon signal, given precessional forcing and spatial patterns of rainfall that are characteristic of modern monsoons (Figs. 7 and 8). In JJA this is the second component of both variables. The mode is associated with precipitation variability of ~2.5 mm/day and temperature variability of ~3°C, with increased precipitation associated with a surface air cooling (note
10 the negative correlation in Table 3, so that positive change in one field is associated with negative change in the other). In both cases, the local magnitude of variability is comparable to that driven by CO₂. In DJF the precessional signal is again apparent in the second mode of precipitation, but the third mode of temperature. This mode is notable, in that it drives changes in simulated precipitation over East Africa (5 mm/day) that exceed CO₂-driven variability. The remaining modes are more complex, and may not represent a clear mode of variability that can be straightforwardly attributed. For instance, the
15 third-order mode of JJA temperature is driven by an interaction between CO₂ and obliquity, but in precipitation can be explained almost exclusively by CO₂.
20

6 Summary and Conclusions

Our ensemble of 50 model runs of the EMIC PLASIM-GENIE has used an early Eocene palaeogeography incorporating recent understanding of the configuration of the continents and ocean gateways, with climate forcing by a randomly selected
25 combination of atmospheric GHG emissions and orbital parameters for each model run. Relationships between forcing parameters and scalar summaries of model results have been derived through linear modelling.

Given the input range of CO₂, our results show that, at the global scale, variability in patterns of surface air temperature is strongly dominated by a single mode of variation with a strong imprint of TPTD, focused in northern winter, that is entirely controlled by CO₂ (> 95% variance in both seasons). We note, however, that regions under the influence of monsoon
30 systems exhibit precession-driven temperature variability that is comparable in magnitude to the variability driven by CO₂ (in large part the high proportion of variance explained by the CO₂ mode arises because the signal is global). In contrast to the unimodal dominance of CO₂ on the modelled global temperature fields, precipitation shows a somewhat more nuanced



response. The first mode of precipitation, while still controlled entirely by CO₂, is much less dominant (maximum 57% variance in DJF cf 21% for PC2). In the second and third spatial modes of precipitation variability, CO₂ is still important, but no more so than orbital parameters, with PC2 controlled more strongly by precession index.

The importance of orbital forcing to precipitation signals is seen more clearly in the OLC and monsoon indices. In spite of large variation in atmospheric CO₂, variation in obliquity accounts for well over half of the variation in high northern latitude ocean-land temperature contrast, and the variation in precession strongly influences seasonal variation in precipitation in tropical Africa and Asia. Our results strongly suggest the presence of monsoons in the early Eocene, but these climatic features would have developed without the effects of orography and high altitude plateau heating which are important factors in the modern south Asian monsoon (Boos and Kuang, 2010).

We note that the relative amplitude of the CO₂-driven modes depends critically on the actual amplitude of CO₂ variability in the period of interest. While the ranges for orbital parameters are well defined, this is less true of CO₂ variability over the Eocene. If atmospheric CO₂ remained within a narrower range throughout the period, and outside of short-lived hyperthermals, the relative influence of CO₂ and orbital inputs might have been more evenly balanced. We have carried out an additional SVD of the 23 ensemble members with CO₂ in the range 700 to 1800 ppm, indicated for the early Eocene by Anagnostou et al. (2016) in a recent study using boron isotopes. This analysis allocates 91% (86%) of the DJF (JJA) SAT variance and 55% (48%) of the DJF (JJA) precipitation variance to the first (CO₂-driven) principal components thus, for global temperature patterns, the orbitally driven components contribute around twice as much variance as in the full ensemble.

Our study of the early Eocene climate and the PETM has shown that variability in orbital parameters can exert significant climatic influence, particularly in regard to tropical temperature and precipitation, and they should not be ignored in modelling studies of climates of the past.

Data Availability

Details on access to the model code, and instructions on compiling the model are given in Holden et al. (2016).

Author Contribution

J. Keery and P. Holden designed and prepared the ensemble configurations and analysed the model outputs with advice from N. Edwards. J. Keery prepared the manuscript with contributions from both co-authors.

Competing Interests

The authors declare that they have no conflict of interest.



Acknowledgements

The authors gratefully acknowledge support from NERC, with funding for project NE/K006223/1.

References

- Abbot, D. S. and Tziperman, E.: A high-latitude convective cloud feedback and equable climates, *Q. J. Roy. Meteor. Soc.*,
5 134, 165-185, doi:10.1002/qj.211, 2008
- Akhmetiev, M. A., Zaporozhets, N. I., Benyamovskiy, V. N., Aleksandrova, G. N., Iakovleva, A. I., and Oreshkina, T. V.:
The Paleogene history of the Western Siberian seaway - A connection of the Peri-Tethys to the Arctic Ocean, *Austrian J.
Earth Sci.*, 105, 50-67, 2012
- Anagnostou, E., John, E. H., Edgar, K. M., Foster, G. L., Ridgwell, A., Inglis, G. N., Pancost, R. D., Lunt, D. J., and
10 Pearson, P. N.: Changing atmospheric CO₂ concentration was the primary driver of early Cenozoic climate, *Nature*, 533,
380-384, doi:10.1038/nature17423, 2016
- Aubry, M.-P., Ouda, K., Dupuis, C., Berggren, W. A., and Couvering, J. A. V.: The Global Standard Stratotype-section and
Point (GSSP) for the base of the Eocene Series in the Dababiya section (Egypt), *Episodes*, 30, 271, 2007
- Backman, J., Jakobsson, M., Frank, M., Sangiorgi, F., Brinkhuis, H., Stickley, C., O'Regan, M., Løvlie, R., Pälike, H.,
15 Spofforth, D., Gattacecca, J., Moran, K., King, J., and Heil, C.: Age model and core-seismic integration for the Cenozoic
Arctic Coring Expedition sediments from the Lomonosov Ridge, *Paleoceanography*, 23, doi:10.1029/2007PA001476, 2008
- Barker, P. and Burrell, J.: The opening of Drake passage, *Mar. Geol.*, 25, 15-34, 1977
- Berger, A., Loutre, M. F., and Tricot, C.: Insolation and Earth's orbital periods, *J. Geophys. Res.-Atmos.*, 98, 10341-10362,
1993
- 20 Boos, W. R. and Kuang, Z.: Dominant control of the South Asian monsoon by orographic insulation versus plateau heating,
Nature, 463, 218-222, doi:10.1038/nature08707, 2010
- Carmichael, M. J., Lunt, D. J., Huber, M., Heinemann, M., Kiehl, J., LeGrande, A., Loftson, C. A., Roberts, C. D., Sagoo,
N., Shields, C., Valdes, P. J., Winguth, A., Winguth, C., and Pancost, R. D.: A model-model and data-model comparison for
the early Eocene hydrological cycle, *Clim. Past*, 12, 455-481, doi:10.5194/cp-12-455-2016, 2016
- 25 Chen, Z., Ding, Z., Yang, S., Zhang, C., and Wang, X.: Increased precipitation and weathering across the Paleocene-Eocene
thermal maximum in central China, *Geochem. Geophys. Geosy.*, 17, 2286-2297, doi:10.1002/2016GC006333, 2016
- Cruz, F. W., Burns, S. J., Karmann, I., Sharp, W. D., Vuille, M., Cardoso, A. O., Ferrari, J. A., Silva Dias, P. L., and Viana,
O.: Insolation-driven changes in atmospheric circulation over the past 116,000 years in subtropical Brazil, *Nature*, 434, 63-
66, doi:10.1038/nature03365, 2005
- 30 Cui, Y., Kump, L. R., Ridgwell, A. J., Charles, A. J., Junium, C. K., Diefendorf, A. F., Freeman, K. H., Urban, N. M., and
Harding, I. C.: Slow release of fossil carbon during the Palaeocene-Eocene Thermal Maximum, *Nat. Geosci.*, 4, 481-485,
doi:10.1038/NCEO1179, 2011



- Dickens, G. R.: Down the rabbit hole: Toward appropriate discussion of methane release from gas hydrate systems during the Paleocene-Eocene thermal maximum and other past hyperthermal events, *Clim. Past*, 7, 831-846, doi.10.5194/cp-7-831-2011, 2011
- Dickson, A. J., Cohen, A. S., and Coe, A. L.: Seawater oxygenation during the Paleocene-Eocene thermal maximum, *Geology*, 40, 639-642, doi.10.1130/G32977.1, 2012
- 5 Dunkley Jones, T., Lunt, D. J., Schmidt, D. N., Ridgwell, A., Sluijs, A., Valdes, P. J., and Maslin, M.: Climate model and proxy data constraints on ocean warming across the Paleocene–Eocene Thermal Maximum, *Earth-Sci. Rev.*, 125, 123-145, doi.10.1016/j.earscirev.2013.07.004, 2013
- Edwards, N. R. and Marsh, R.: Uncertainties due to transport-parameter sensitivity in an efficient 3-D ocean-climate model, *Clim. Dynam.*, 24, 415-433, doi.10.1007/s00382-004-0508-8, 2005
- 10 Exon, N. F., Kennett, J. P., and Malone, M. J.: Leg 189 synthesis: Cretaceous–Holocene history of the Tasmanian Gateway. In: *Proceedings of the Ocean Drilling Program, Scientific Results*, 189, Exon, N. F., Kennett, J. P., and Malone, M. J. (Eds.), Ocean Drilling Program, College Station, TX 2004.
- Fraedrich, K.: A suite of user-friendly global climate models: hysteresis experiments, *Eur. Phys. J. Plus*, 127, 1-9, doi.10.1140/epjp/i2012-12053-7, 2012
- 15 Fraedrich, K., Kirk, E., Luksch, U., and Lunkeit, F.: The portable university model of the atmosphere (PUMA): Storm track dynamics and low-frequency variability, *Meteorol. Z.*, 14, 735-745, doi.10.1127/0941-2948/2005/0074, 2005
- Gehler, A., Gingerich, P. D., and Pack, A.: Temperature and atmospheric CO₂ concentration estimates through the PETM using triple oxygen isotope analysis of mammalian bioapatite, *P. Natl. Acad. Sci. USA*, doi: 10.1073/pnas.1518116113, 2016. 201518116, doi.10.1073/pnas.1518116113, 2016
- 20 Gibbs, S. J., Bown, P. R., Sessa, J. A., Bralower, T. J., and Wilson, P. A.: Nannoplankton extinction and origination across the Paleocene-Eocene thermal maximum, *Science*, 314, 1770-1773, 2006
- Gough, D. O.: Solar interior structure and luminosity variations, *Sol. Phys.*, 74, 21-34, doi.10.1007/BF00151270, 1981
- Hannachi, A.: *A primer for EOF analysis of climate data*. University of Reading, Reading, 2004.
- 25 Herold, N., Buzan, J., Seton, M., Goldner, A., Green, J., Müller, R., Markwick, P., and Huber, M.: A suite of early Eocene (~55 Ma) climate model boundary conditions, *Geosci. Model Dev.*, 7, 2077-2090, doi.10.5194/gmd-7-2077-2014, 2014
- Hibler III, W.: A dynamic thermodynamic sea ice model, *J. Phys. Oceanogr.*, 9, 815-846, 1979
- Hilgen, F. J., Kuiper, K. F., and Lourens, L. J.: Evaluation of the astronomical time scale for the Paleocene and earliest Eocene, *Earth Planet. Sc. Lett.*, 300, 139-151, doi.10.1016/j.epsl.2010.09.044, 2010
- 30 Hinnov, L. A. and Hilgen, F. J.: Chapter 4 - Cyclostratigraphy and Astrochronology. In: *The Geologic Time Scale 2012*, Gradstein, F. M., Ogg, J. G., Schmitz, M. D., and Ogg, G. M. (Eds.), Elsevier, Boston, 2012.
- Holden, P. B., Edwards, N. R., Fraedrich, K., Kirk, E., Lunkeit, F., and Zhu, X.: PLASIM–GENIE v1.0: a new intermediate complexity AOGCM, *Geosci. Model Dev.*, 9, 3347-3361, doi.10.5194/gmd-9-3347-2016, 2016



- Holden, P. B., Edwards, N. R., Garthwaite, P. H., and Wilkinson, R. D.: Emulation and interpretation of high-dimensional climate model outputs, *J. Appl. Stat.*, 42, 2038-2055, doi:10.1080/02664763.2015.1016412, 2015
- Huber, M.: Progress in greenhouse climate modeling. In: *Reconstructing Earth's Deep-Time Climate - The State of the Art in 2012*, Ivany, L. C. and Huber, B. T. (Eds.), The Paleontological Society, Boulder, CO, 2012.
- 5 Huber, M. and Caballero, R.: The early Eocene equable climate problem revisited, *Clim. Past*, 7, 603-633, doi:10.5194/cp-7-603-2011, 2011
- Jain, S., Lall, U., and Mann, M. E.: Seasonality and interannual variations of Northern Hemisphere temperature: Equator-to-pole gradient and ocean-land contrast, *J. Climate*, 12, 1086-1100, 1999
- Jenkyns, H. C.: Geochemistry of oceanic anoxic events, *Geochem. Geophys. Geosy.*, 11, doi:10.1029/2009GC002788, 2010
- 10 Jones, P. D. and Mann, M. E.: Climate over past millennia, *Rev. Geophys.*, 42, 2004
- Karoly, D. J. and Braganza, K.: Identifying global climate change using simple indices, *Geophys. Res. Lett.*, 28, 2205-2208, 2001
- Kennett, J. and Stott, L.: Abrupt deep-sea warming, palaeoceanographic changes and benthic extinctions at the end of the Palaeocene, *Nature*, 353, 225-229, doi:10.1038/353225a0, 1991
- 15 Laskar, J., Fienga, A., Gastineau, M., and Manche, H.: La2010: a new orbital solution for the long-term motion of the Earth, *Astron. Astrophys.*, 532, A89, doi:10.1051/0004-6361/201116836, 2011
- Lauretano, V., Littler, K., Polling, M., Zachos, J. C., and Lourens, L. J.: Frequency, magnitude and character of hyperthermal events at the onset of the Early Eocene Climatic Optimum, *Clim. Past*, 11, 1313-1324, doi:10.5194/cp-11-1313-2015, 2015
- 20 Laurin, J., Meyers, S. R., Galeotti, S., and Lanci, L.: Frequency modulation reveals the phasing of orbital eccentricity during Cretaceous Oceanic Anoxic Event II and the Eocene hyperthermals, *Earth Planet. Sc. Lett.*, 442, 143-156, doi:10.1016/j.epsl.2016.02.047, 2016
- Lourens, L. J., Sluijs, A., Kroon, D., Zachos, J. C., Thomas, E., Röhl, U., Bowles, J., and Raffi, I.: Astronomical pacing of late Palaeocene to early Eocene global warming events, *Nature*, 435, 1083-1087, doi:10.1038/nature03814, 2005
- 25 Lunt, D., Elderfield, H., Pancost, R., Ridgwell, A., Foster, G., Haywood, A., Kiehl, J., Sgouros, N., Shields, C., and Stone, E.: Warm climates of the past—a lesson for the future?, *Philos. T. R. Soc.-A*, 371, 20130146, doi:10.1098/rsta.2013.0146, 2013
- Lunt, D. J., Dunkley Jones, T., Heinemann, M., Huber, M., LeGrande, A., Winguth, A., Loptson, C., Marotzke, J., Roberts, C., and Tindall, J.: A model–data comparison for a multi-model ensemble of early Eocene atmosphere–ocean simulations: EoMIP, *Clim. Past*, 8, 1717-1736, doi:10.5194/cp-8-1717-2012, 2012
- 30 Lunt, D. J., Farnsworth, A., Loptson, C., Foster, G. L., Markwick, P., O'Brien, C. L., Pancost, R. D., Robinson, S. A., and Wrobel, N.: Palaeogeographic controls on climate and proxy interpretation, *Clim. Past*, 12, 1181-1198, doi:10.5194/cp-12-1181-2016, 2016
- Lunt, D. J., Ridgwell, A., Sluijs, A., Zachos, J., Hunter, S., and Haywood, A.: A model for orbital pacing of methane hydrate destabilization during the Palaeogene, *Nat. Geosci.*, 4, 775-778, doi:10.1038/ngeo1266, 2011



- Marincovich, L., Brouwers, E. M., Hopkins, D. M., and McKenna, M. C.: Late Mesozoic and Cenozoic paleogeographic and paleoclimatic history of the Arctic Ocean Basin, based on shallow-water faunas and terrestrial vertebrates. In: *The Geology of North America, L: The Arctic Ocean Region*, Grantz, A., Sweeney, J. F., and Johnson, G. L. (Eds.), Geological Society of America, 1990.
- 5 Marsh, R., Müller, S., Yool, A., and Edwards, N.: Incorporation of the C-GOLDSTEIN efficient climate model into the GENIE framework: "eb_go_gs" configurations of GENIE, *Geosci. Model Dev.*, 4, 957-992, doi.10.5194/gmd-4-957-2011, 2011
- McInerney, F. A. and Wing, S. L.: The Paleocene-Eocene Thermal Maximum: A perturbation of carbon cycle, climate, and biosphere with implications for the future, *Annu. Rev. Earth Pl. Sc.*, 39, 489-516, doi.10.1146/annurev-earth-040610-10 133431, 2011
- McKay, M. D., Beckman, R. J., and Conover, W. J.: A comparison of three methods for selecting values of input variables in the analysis of output from a computer code, *Technometrics*, 21, 239-245, 1979
- O'Regan, M., Moran, K., Backman, J., Jakobsson, M., Sangiorgi, F., Brinkhuis, H., Pockalny, R., Skelton, A., Stickley, C., and Koç, N.: Mid-Cenozoic tectonic and paleoenvironmental setting of the central Arctic Ocean, *Paleoceanography*, 23, 15 doi.10.1029/2007PA001559, 2008
- Peixoto, J. P. and Oort, A. H.: *Physics of Climate*, American Institute of Physics, New York, 1992.
- Penman, D. E.: Silicate weathering and North Atlantic silica burial during the Paleocene-Eocene Thermal Maximum, *Geology*, doi: 10.1130/G37704.1, 2016. G37704. 37701, doi.10.1130/G37704.1, 2016
- Penman, D. E., Hönisch, B., Zeebe, R. E., Thomas, E., and Zachos, J. C.: Rapid and sustained surface ocean acidification 20 during the Paleocene-Eocene Thermal Maximum, *Paleoceanography*, 29, 357-369, doi.10.1002/2014PA002621, 2014
- Radionova, E. and Khokhlova, I.: Was the North Atlantic connected with the Tethys via the Arctic in the early Eocene? Evidence from siliceous plankton, *GFF*, 122, 133-134, doi.10.1080/11035890001221133, 2000
- Rougier, J.: Probabilistic inference for future climate using an ensemble of climate model evaluations, *Climatic Change*, 81, 247-264, doi.10.1007/s10584-006-9156-9, 2007
- 25 Ruddiman, W. F.: Orbital changes and climate, *Quaternary Sci. Rev.*, 25, 3092-3112, doi.10.1016/j.quascirev.2006.09.001, 2006
- Semtner Jr, A. J.: A model for the thermodynamic growth of sea ice in numerical investigations of climate, *J. Phys. Oceanogr.*, 6, 379-389, 1976
- Sexton, P. F., Norris, R. D., Wilson, P. A., Pälike, H., Westerhold, T., Röhl, U., Bolton, C. T., and Gibbs, S.: Eocene global 30 warming events driven by ventilation of oceanic dissolved organic carbon, *Nature*, 471, 349-352, doi.10.1038/nature09826, 2011
- Sijp, W. P., Anna, S., Dijkstra, H. A., Flögel, S., Douglas, P. M., and Bijl, P. K.: The role of ocean gateways on cooling climate on long time scales, *Global Planet. Change*, 119, 1-22, doi.10.1016/j.gloplacha.2014.04.004, 2014



- Slattery, J. S., Cobban, W. A., McKinney, K. C., Harries, P. J., and Sandness, A. L.: Early Cretaceous to Paleocene paleogeography of the Western Interior Seaway: The interaction of eustasy and tectonism. In: *Cretaceous Conference: Evolution and Revolution*, Bingle-Davis, M. (Ed.), Wyoming Geological Association, Casper, WY, 2015.
- Sloan, L. C. and Barron, E. J.: "Equable" climates during Earth history?, *Geology*, 18, 489-492, 1990
- 5 Sluijs, A., Schouten, S., Pagani, M., Woltering, M., Brinkhuis, H., Damsté, J. S. S., Dickens, G. R., Huber, M., Reichert, G.-J., and Stein, R.: Subtropical Arctic Ocean temperatures during the Palaeocene/Eocene thermal maximum, *Nature*, 441, 610-613, doi.10.1038/nature04668, 2006
- Sluijs, A., Zachos, J. C., and Zeebe, R. E.: Constraints on hyperthermals, *Nat. Geosci.*, 5, 231-231, doi.10.1038/ngeo1423, 2012
- 10 Smith, M. E., Carroll, A. R., Scott, J. J., and Singer, B. S.: Early Eocene carbon isotope excursions and landscape destabilization at eccentricity minima: Green River Formation of Wyoming, *Earth Planet. Sc. Lett.*, 403, 393-406, doi.10.1016/j.epsl.2014.06.024, 2014
- Trenberth, K. E., Hurrell, J. W., and Stepaniak, D. P.: The Asian monsoon: Global perspectives. In: *The Asian Monsoon*, Wang, B. (Ed.), Springer, New York, 2006.
- 15 Wang, B. and Fan, Z.: Choice of South Asian summer monsoon indices, *B. Am. Meteorol. Soc.*, 80, 629, 1999
- Weber, S. L.: The utility of Earth system Models of Intermediate Complexity (EMICs), *Wiley Interdisciplinary Reviews: Climate Change*, 1, 243-252, doi.10.1002/wcc.24, 2010
- Westerhold, T., Röhl, U., and Laskar, J.: Time scale controversy: Accurate orbital calibration of the early Paleogene, *Geochem. Geophys. Geosy.*, 13, doi.10.1029/2012GC004096, 2012
- 20 Westerhold, T., Röhl, U., McCarren, H. K., and Zachos, J. C.: Latest on the absolute age of the Paleocene–Eocene Thermal Maximum (PETM): new insights from exact stratigraphic position of key ash layers+ 19 and– 17, *Earth Planet. Sc. Lett.*, 287, 412-419, doi.10.1016/j.epsl.2009.08.027, 2009
- Williamson, M. S., Lenton, T. M., Shepherd, J. G., and Edwards, N. R.: An efficient numerical terrestrial scheme (ENTS) for Earth system modelling, *Ecol. Model.*, 198, 362-374, doi.10.1016/j.ecolmodel.2006.05.027, 2006
- 25 Wing, S. L. and Greenwood, D. R.: Fossils and fossil climate: the case for equable continental interiors in the Eocene, *Philos. T. R. Soc.-B*, 341, 243-252, 1993
- Wyss, G. D. and Jorgensen, K. H.: *A User's Guide to LHS: Sandia's Latin Hypercube Sampling Software*. Sandia National Laboratories, Albuquerque, NM, 1998.
- Zachos, J. C., Bohaty, S. M., John, C. M., McCarren, H., Kelly, D. C., and Nielsen, T.: The Palaeocene–Eocene carbon isotope excursion: constraints from individual shell planktonic foraminifer records, *Philos. T. R. Soc.-A*, 365, 1829-1842, doi.10.1098/rsta.2007.2045, 2007
- Zachos, J. C., Röhl, U., Schellenberg, S. A., Sluijs, A., Hodell, D. A., Kelly, D. C., Thomas, E., Nicolo, M., Raffi, I., Lourens, L. J., McCarren, H., and Kroon, D.: Rapid Acidification of the Ocean during the Paleocene-Eocene Thermal Maximum, *Science*, 308, 1611-1615, doi.10.2307/3841617, 2005



Zachos, J. C., Wara, M. W., Bohaty, S., Delaney, M. L., Petrizzo, M. R., Brill, A., Bralower, T. J., and Premoli-Silva, I.: A transient rise in tropical sea surface temperature during the Paleocene-Eocene thermal maximum, *Science*, 302, 1551-1554, 2003

5 Zeebe, R. E., Ridgwell, A., and Zachos, J. C.: Anthropogenic carbon release rate unprecedented during the past 66 million years, *Nat. Geosci.*, 9, 325–329, doi.10.1038/ngeo2681, 2016

Zeebe, R. E. and Zachos, J. C.: Long-term legacy of massive carbon input to the Earth system: Anthropocene versus Eocene, *Philos. T. R. Soc.-A*, 371, 20120006, doi.10.1098/rsta.2012.0006, 2013



Table 1 Uniform ranges for forcing and dummy parameters

	min	max
pCO₂ (ppm)	280	3000
Precession (°)	0	360
Obliquity (°)	22.0	24.5
Eccentricity (-)	0.00	0.06
Dummy (-)	0	1

Table 2 R² correlation between PC scores from SVD and PC scores emulated with the linear models.

	PC1	PC2	PC3
DJF_temperature	0.95	0.58	0.75
JJA_temperature	0.97	0.97	0.72
DJF_precipitation	0.97	0.92	0.64
JJA_precipitation	0.99	0.99	0.89

5

Table 3 Total effects of forcing parameters on simple scalar metrics.

	CO ₂	Eccentricity	Obliquity	Precession
MAT	0.996	0.002	0.000	0.002
N. seasonality	0.873	0.025	0.013	0.088
N. winter TPTD	0.974	0.009	0.010	0.007
N. summer TPTD	0.084	0.046	0.640	0.229
S. winter POLC	0.996	0.000	0.000	0.004
N. winter POLC	0.268	0.018	0.659	0.055
Asian monsoon index	0.087	0.078	0.073	0.762
African monsoon index	0.061	0.137	0.010	0.792

10



Table 4 R^2 correlation values for PC scores for temperature and precipitation in DJF and JJA. Values where $R^2 \geq 0.5$ are shown in red.

		DJF_precipitation		
		PC1	PC2	PC3
DJF_temperature	PC1	0.993	-0.004	-0.080
	PC2	-0.067	-0.364	-0.864
	PC3	0.005	0.783	-0.354
		JJA_precipitation		
		PC1	PC2	PC3
JJA_temperature	PC1	0.976	0.091	0.157
	PC2	0.098	-0.947	0.082
	PC3	-0.180	-0.049	0.795

5 Table 5 R^2 correlation values for forcing factors and PC scores. Values where $R^2 \geq 0.5$ are shown in red.

		precession		
		CO ₂	index	obliquity
DJF_temperature	PC1	-0.859	-0.018	-0.057
	PC2	0.381	-0.087	-0.354
	PC3	0.038	-0.924	0.311
JJA_temperature	PC1	-0.899	0.178	-0.066
	PC2	-0.018	-0.875	0.362
	PC3	0.342	0.056	-0.239
DJF_precipitation	PC1	-0.867	0.003	-0.025
	PC2	-0.198	-0.820	0.044
	PC3	-0.278	0.465	0.164
JJA_precipitation	PC1	-0.953	0.065	0.008
	PC2	-0.070	0.960	-0.131
	PC3	0.219	0.191	-0.029

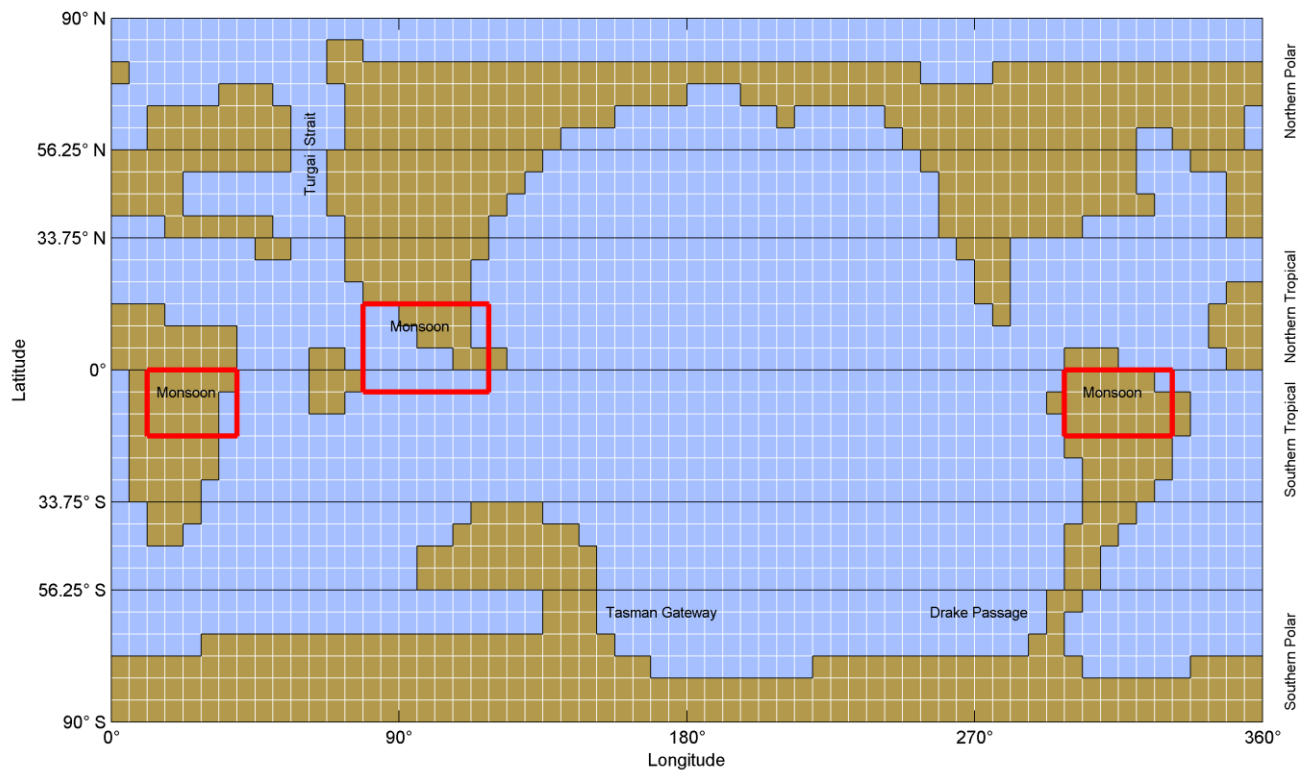


Figure 1: Eocene palaeogeography and geographic areas used to determine simple metric values

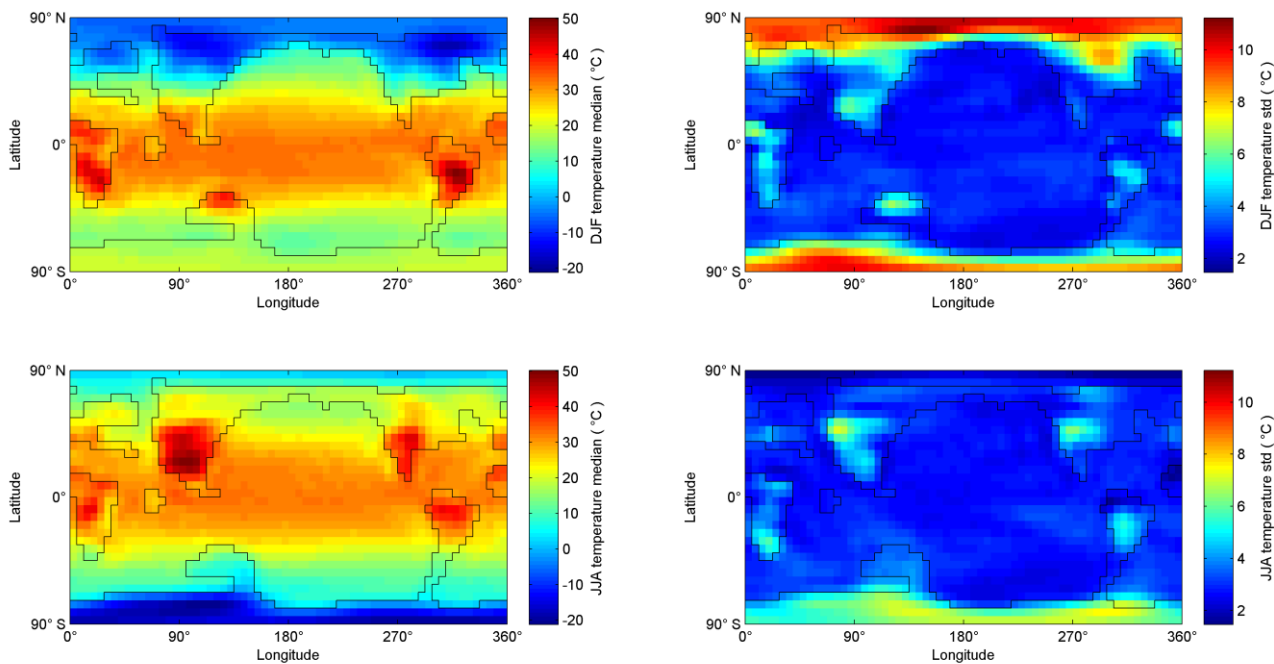


Figure 2: Ensemble temperature medians (left column) and standard deviations (right column) in DJF (top row) and JJA (bottom row).

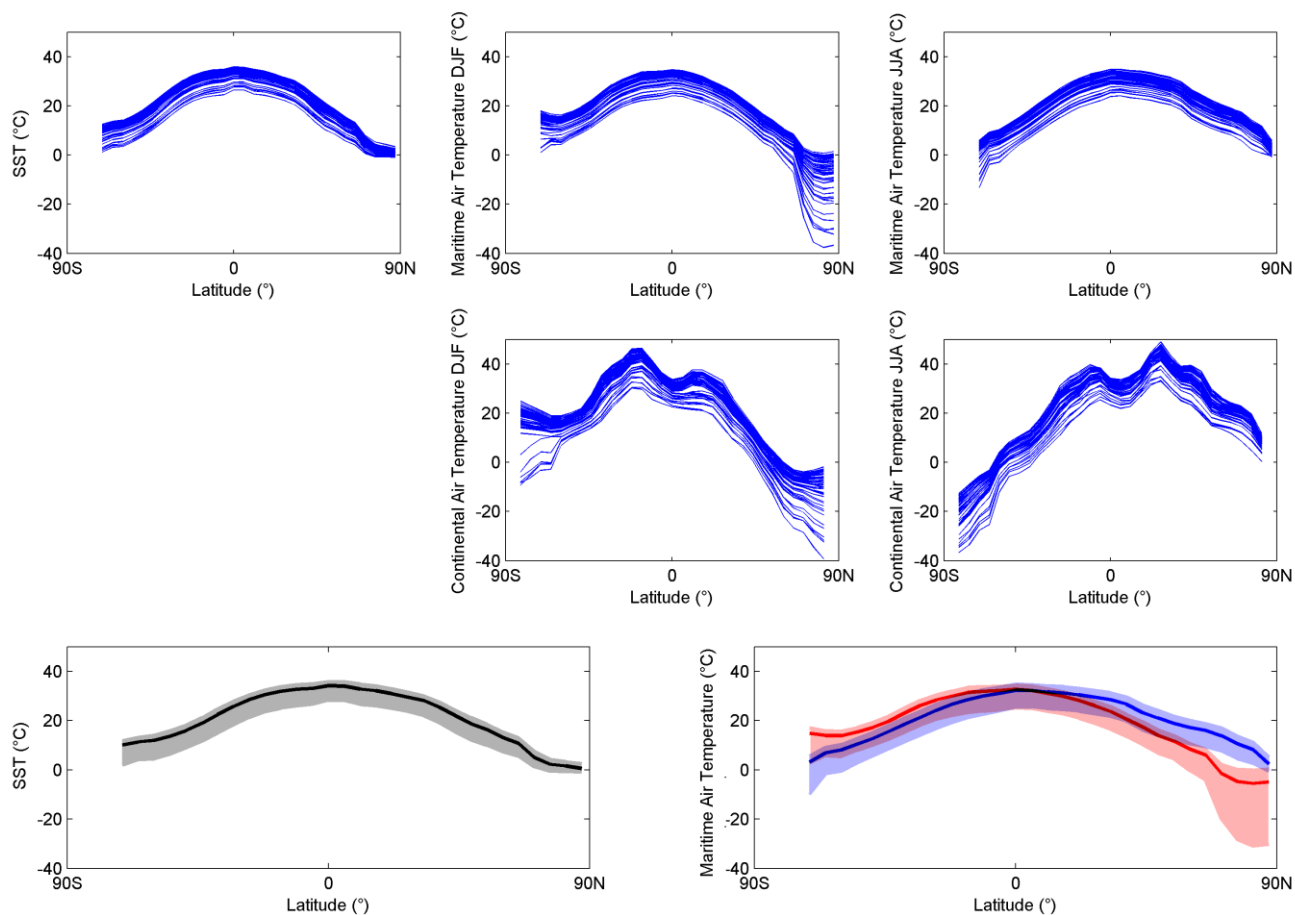


Figure 3: Top: full ensemble distributions of mean latitude values of global annual mean sea surface temperature (SST), with mean latitude maritime surface air temperature in DJF and JJA.

Middle: mean latitude continental surface air temperature in DJF and JJA.

- 5 **Bottom: ensemble medians and 5% and 95% percentiles of global annual mean SST, and maritime surface air temperature in DJF (red) and JJA (blue).**

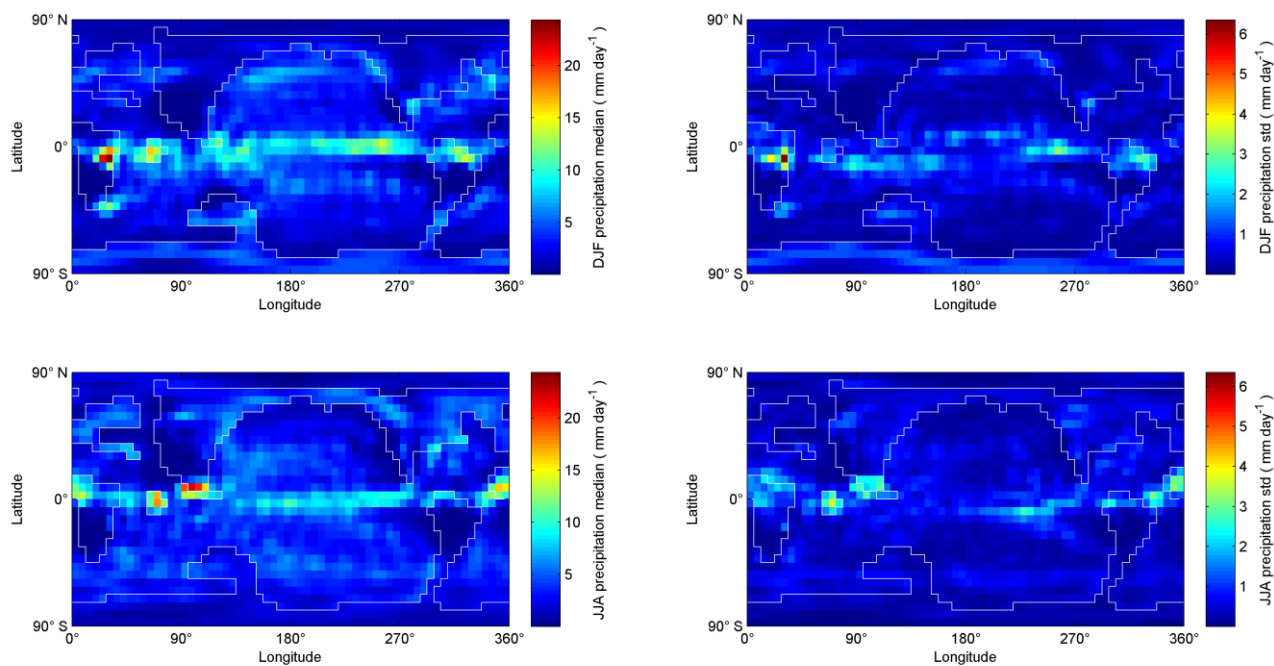


Figure 4: Ensemble precipitation medians (left column) and standard deviations (right column) in DJF (top row) and JJA (bottom row).

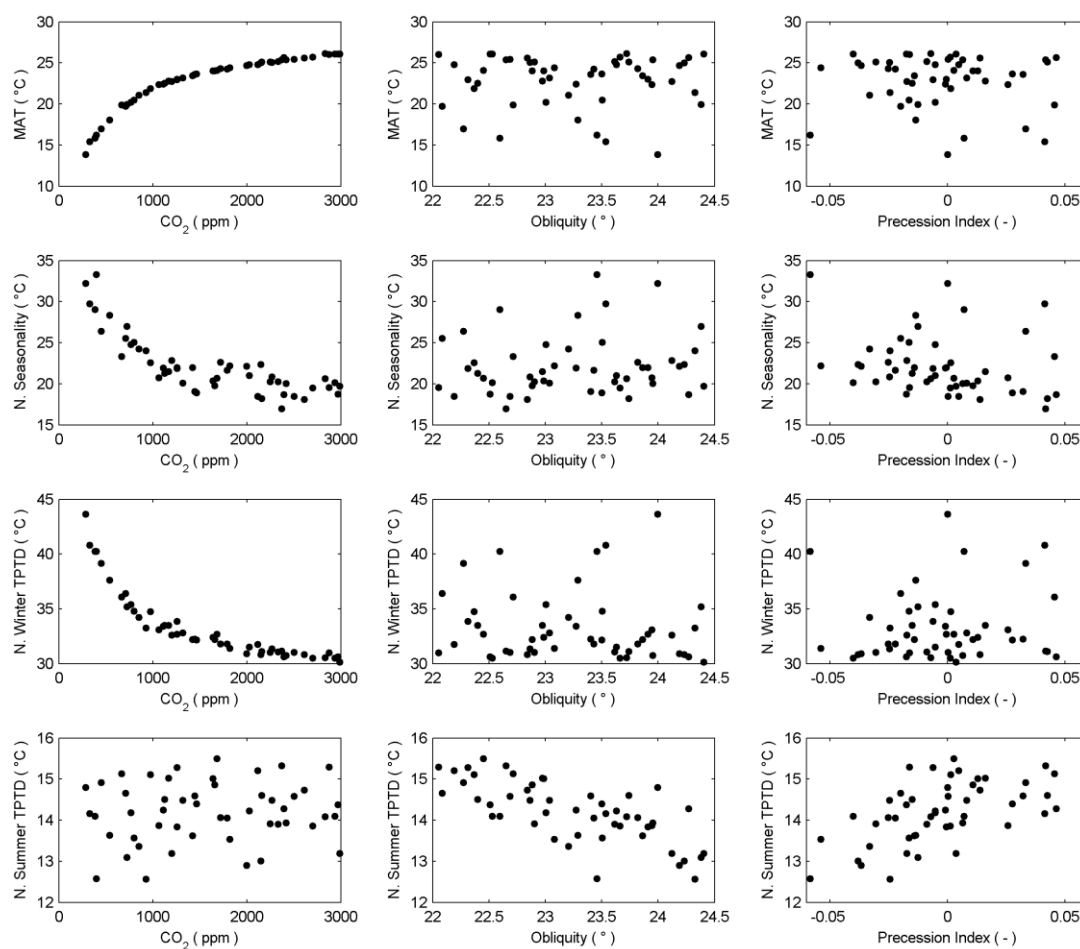


Figure 5: Correlation between three forcing factors CO₂, obliquity and precession index (in columns from left to right), and the simple metrics MAT, northern seasonality, northern winter tropical-polar temperature difference and northern summer tropical-polar temperature difference (in rows from top to bottom).

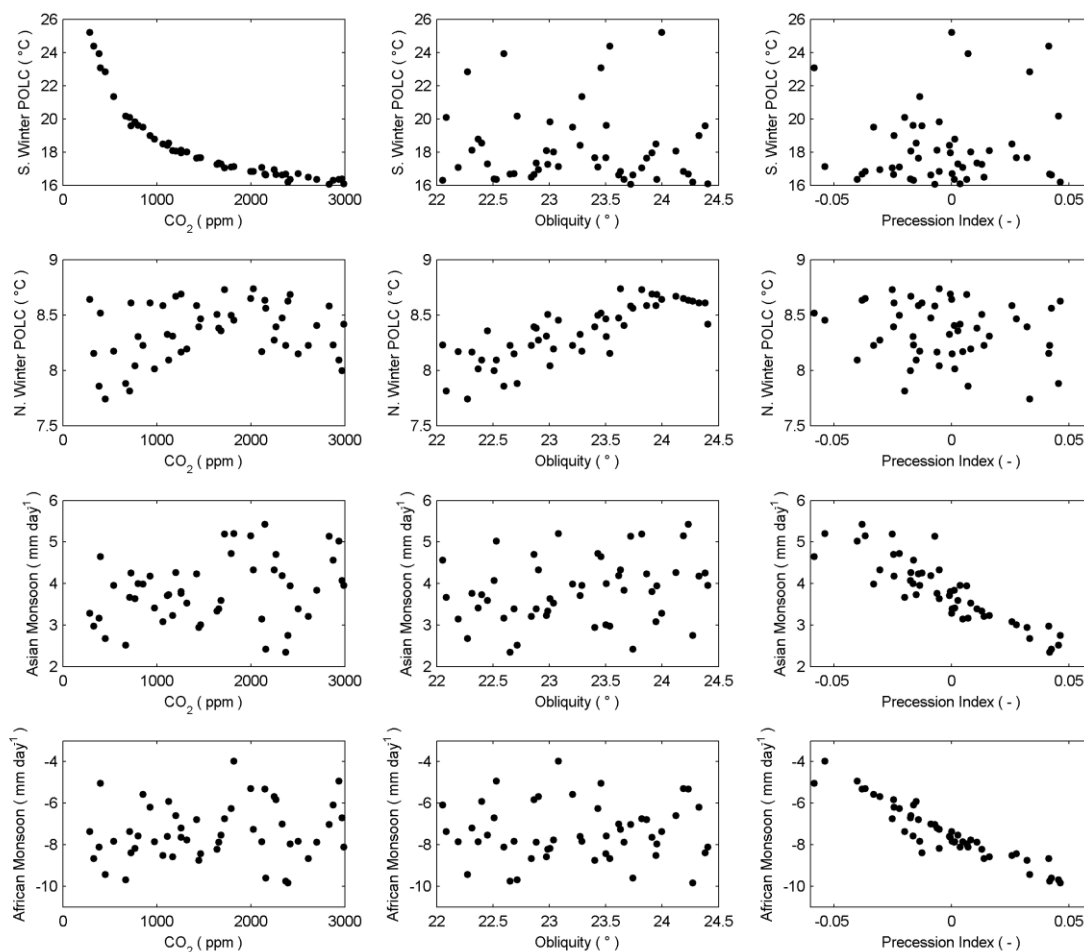


Figure 6: Correlation between three forcing factors CO₂, obliquity and precession index (in columns from left to right), and the simple metrics southern winter polar OLC, northern winter polar OLC, Asian monsoon index, and African monsoon index (in rows from top to bottom).

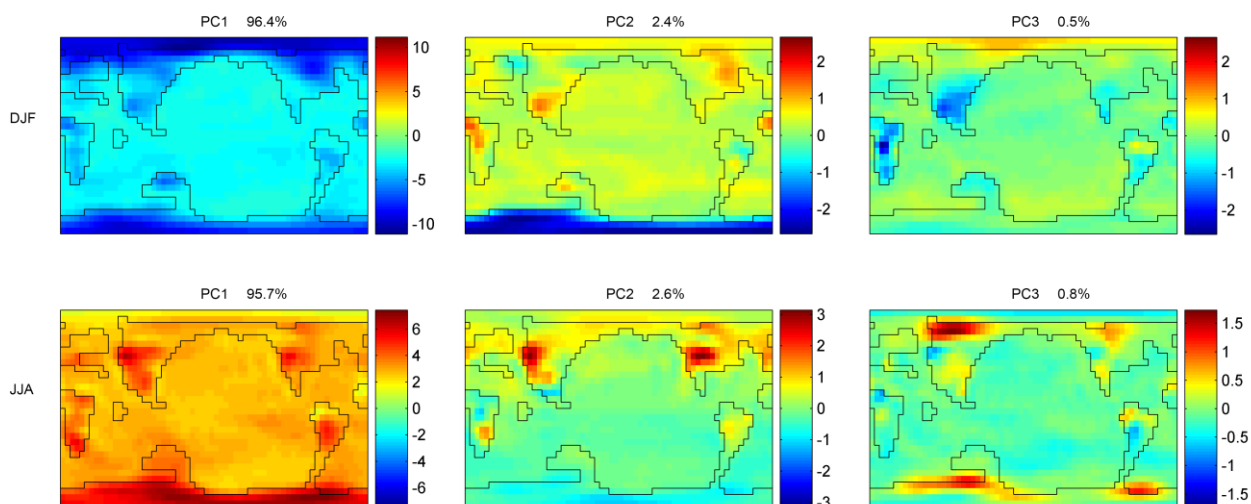


Figure 7: The first three principal components of DJF_temperature (top row) and JJA_temperature (bottom row). Percentages of variance explained by each principal component are shown above each plot.

5

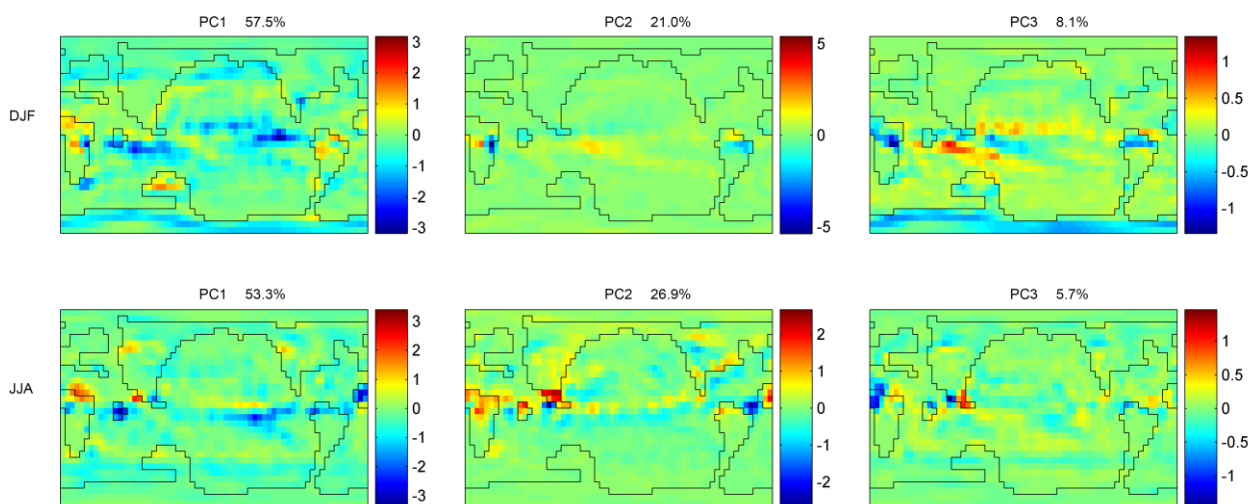


Figure 8: The first three principal components of DJF_precipitation (top row) and JJA_precipitation (bottom row). Percentages of variance explained by each principal component are shown above each plot.

10

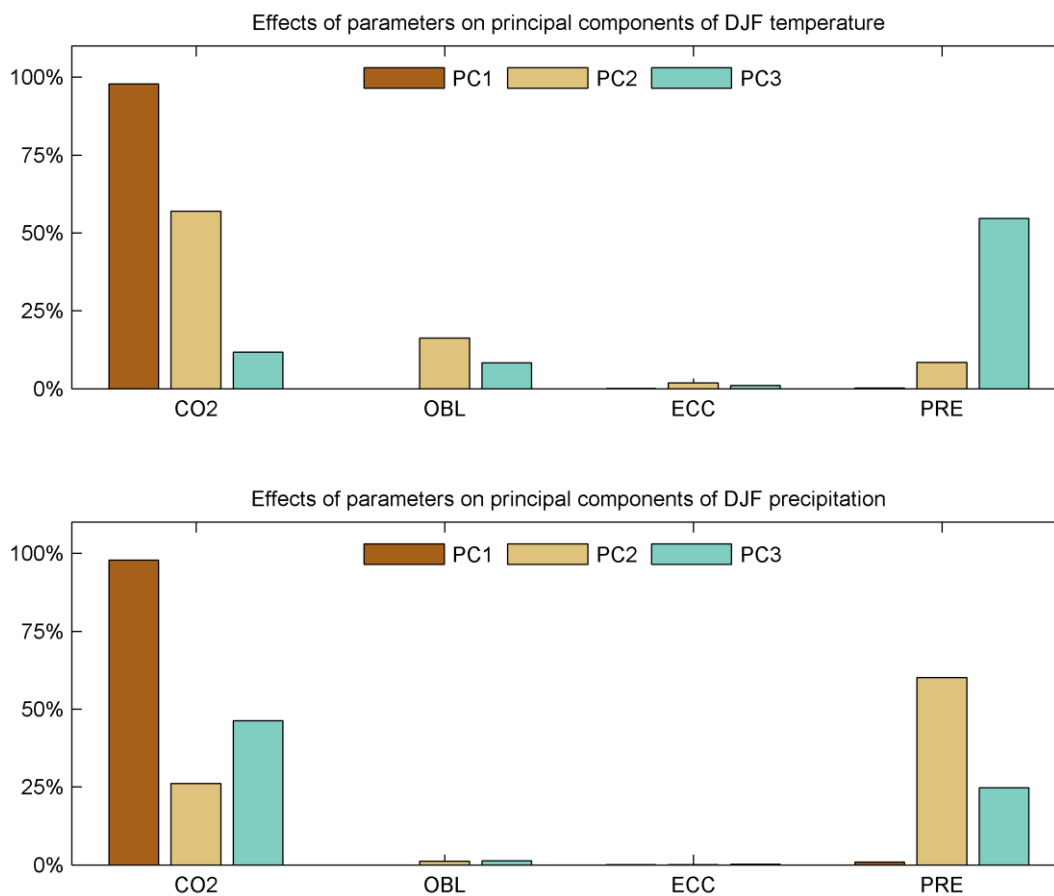


Figure 9: Main effects of forcing parameters on the first three principal components of DJF_temperature (top row) and DJF_precipitation (bottom row).

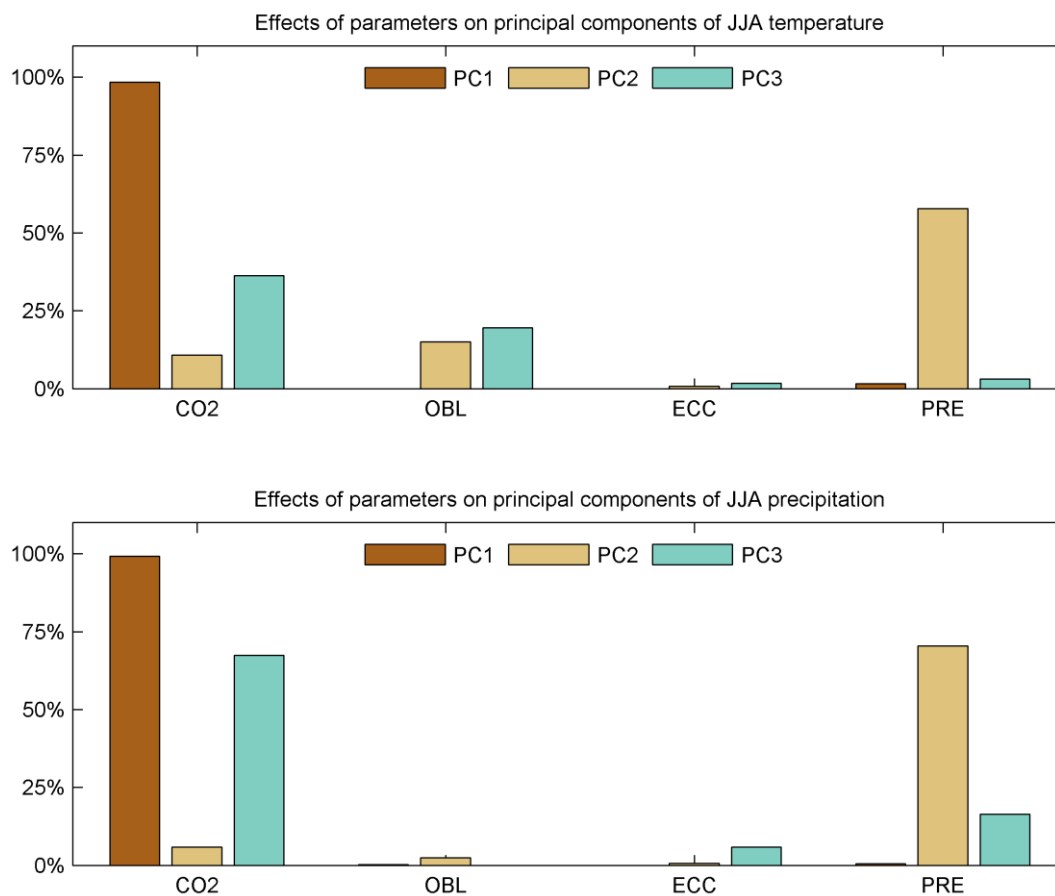


Figure 10: Main effects of forcing parameters on the first three principal components of JJA_temperature (top row) and JJA_precipitation (bottom row).